



ChemComm

Engineering of CdS-chain arrays assembled through S...S interactions in 1D semiconductive coordination polymers

Journal:	<i>ChemComm</i>
Manuscript ID	CC-COM-11-2023-005689.R1
Article Type:	Communication

SCHOLARONE™
Manuscripts

COMMUNICATION

Engineering of CdS-chain arrays assembled through S...S interactions in 1D semiconductive coordination polymers

Received 00th January 20xx,
Accepted 00th January 20xx

Asuka Nishibe,^a Ryohei Akiyoshi,^{*a} Akinori Saeki,^b Kazuyoshi Ogasawara,^a Takaaki Tsuruoka^c and Daisuke Tanaka^{*a}

DOI: 10.1039/x0xx00000x

One-dimensional (1D) Cd(II) coordination polymers [Cd(*x*-SPhOMe)₂]_n (*x* = *ortho*, *meta*, and *para*; HSPHOMe = methoxybenzenethiol) containing inorganic 1D (–Cd–S–)_n chains were synthesized. Among these, the KGF-31 polymer bearing *para*-SPhOMe featured a three-strand chain structure assembled via interchain S...S interactions and exhibited high photoconductivity and longevity.

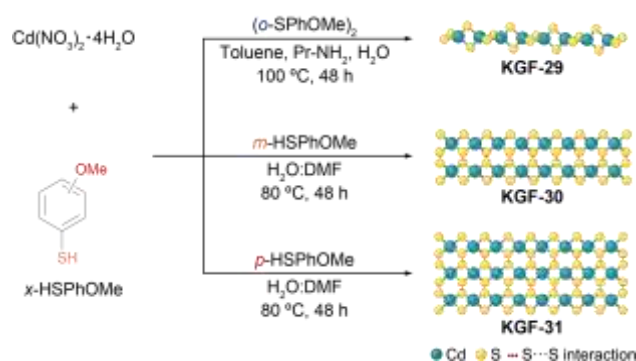
Sulfur-coordinated coordination polymers (S-CPs)¹ have attracted considerable attention in recent years owing to their potential applications in photocatalysis,² chemiresistive sensing,³ and electronic devices.⁴ The inorganic (–M–S–)_n structures formed in the S-CPs give rise to unique optoelectronic properties such as visible light absorption and high charge mobility.⁵ Although an earlier study clearly demonstrated that the structure of inorganic (–M–S–)_n moieties have a significant influence on the resulting semiconductive properties, a weak intermolecular interaction between inorganic (–M–S–)_n networks is neglected despite the impact of the assembled structures on the charge mobility. In typical molecular conductors such as tetrathiafulvalene (TTF) derivatives, S...S interactions between TTF units are crucial for charge delocalization.⁶ The assembly of inorganic (–M–S–)_n structures via S...S interactions in S-CPs is therefore expected to endow further unique optoelectronic properties.

In this study, we used Cd(II) as a metal ion because inorganic CdS exhibits excellent semiconductive properties.⁷ To date, only a few Cd(II) S-CPs with photocatalytic applications have been reported.⁸ For example, Cd(II) S-CP containing 1,3,4-thiadiazole-2,5-dithiol ligand exhibits an efficient photocatalytic H₂ evolution.^{2a} Despite its excellent semiconductive properties,

the relationship between the crystal structures and semiconductive properties of Cd(II) S-CPs has not been systematically investigated.

In this study, we systematically synthesized semiconductive Cd(II) S-CPs using methoxybenzenethiol-isomers. Benzenethiol-derived ligands have easily modifiable structures that facilitate the fine-tuning of assembled structure and the (–M–S–)_n structure.⁹ By changing the position of the methoxy substituents, we synthesized three semiconductive Cd(II) S-CPs with 1D inorganic (–Cd–S–)_n structures assembled through S...S interactions: [Cd(*x*-SPhOMe)₂]_n (*x* = *ortho* (KGF-29), *meta* (KGF-30), and *para* (KGF-31); HSPHOMe = methoxybenzenethiol) (Scheme 1). KGF-29 formed an isolated 1D structure containing 1D (–Cd–S–)_n chains, whereas KGF-30 and KGF-31 formed two- and three-strand chain structures, respectively, via S...S interactions between 1D (–Cd–S–)_n chains. KGF-31, which has three-strand chains, exhibits superior photoconductivity and longevity than KGF-29 and KGF-30.

Colorless needle-like crystals of KGF-29 were obtained from Cd(NO₃)₂·4H₂O and (*o*-SPhOMe)₂ (dimerized *o*-HSPHOMe through disulfide bond) via solvothermal synthesis at 100 °C for 96 h.¹⁰ KGF-29 crystallized in the triclinic *P* $\bar{1}$ space group (Table S1), with an asymmetric unit consisting of one Cd(II) ion and two *o*-SPhOMe groups (Fig. S1a). The Cd(II) center was coordinated by four *o*-HSPHOMe groups through the S atoms, yielding tetrahedral [CdS₄] coordination units (Fig. S2a). The Cd–S bond lengths (2.584–2.601 Å) are comparable to those in inorganic



Scheme 1. Synthesis of [Cd(*x*-SPhOMe)₂]_n (*x* = *ortho* (KGF-29), *meta* (KGF-30), *para* (KGF-31)).

^a Department of Chemistry, School of Science, Kwansai Gakuin University, 1 Gakuen Uegahara, Sanda, Hyogo 669-1330, Japan

^b Department of Applied Chemistry, Graduate School of Engineering, Osaka University, 2-1 Yamadaoka, Suita, Osaka 565-0871, Japan

^c Department of Nanobiochemistry, Frontiers of Innovative Research in Science and Technology (FIRST), Konan University, Kobe, Hyogo 650-0047, Japan

Electronic Supplementary Information (ESI) available: Crystallographic data, XPS results, comparison of experimental and simulated PXRD patterns, SEM and EDS images, TG analyses, summary of optical band gap energies, PYS results, exponential decay fitting for TRMC spectra, List of TRMC results, VBM and CBM distribution, PDOS ratio. See DOI: 10.1039/x0xx00000x

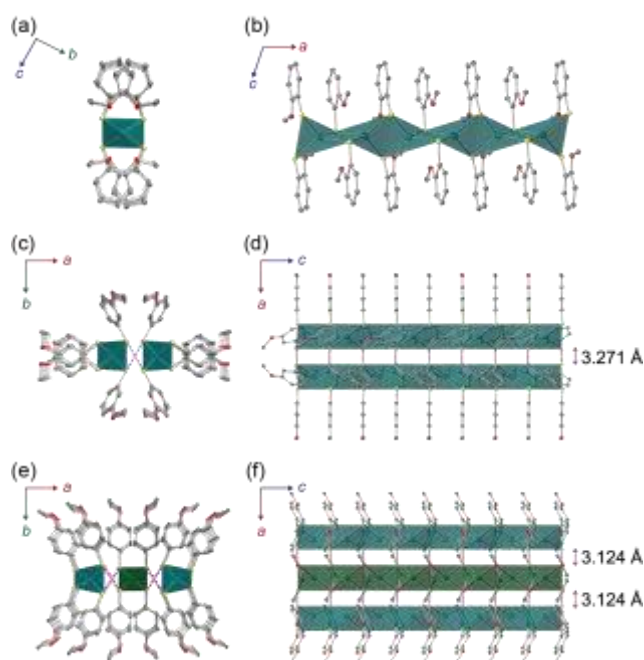


Fig. 1. Crystal structures of **KGF-29**, **KGF-30**, and **KGF-31**. 1D chain structures of (a)(b) **KGF-29**, (c)(d) **KGF-30**, and (e)(f) **KGF-31**. Color code: green; Cd, yellow; S, grey; C, red; O, H atoms are omitted for clarity. S...S interactions are colored in purple.

CdS (Table S2).⁷ The S atoms acted as a μ_2 -S atom (Fig. S3a) and connected to the adjacent [CdS₄] tetrahedron with repeated edge-sharing (Fig. S4a). Consequently, **KGF-29** adopted a 1D structure containing inorganic (–Cd–S–)_n chains along the *a*-axis (Fig. 1a, b). The resulting 1D structure was assembled by weak van der Waals (vdW) interactions between the 1D chains (Fig. S5a).

Single crystals of **KGF-30** were obtained from Cd(NO₃)₂·4H₂O and *m*-HSPHOMe by solvothermal synthesis at 80 °C for 48 h. **KGF-30** crystallized in the orthorhombic *Pccn* space group (Table S1), with an asymmetric unit consisting of one Cd(II) ion and two *m*-SPhOMe ligands (Fig. S1b). Like **KGF-29**, **KGF-30** featured [CdS₄] tetrahedra with a central Cd(II) atom coordinated by four S atoms from *m*-SPhOMe ligands (Fig. S2b). The Cd–S bond lengths (2.561–2.593 Å) were similar to those of **KGF-29** (Table S2). The S atoms of **KGF-30** are also μ_2 -S atom (Fig. S3b) that form a 1D structure with repeated edge-sharing of [CdS₄] tetrahedra along the *c*-axis (Fig. 1c, d, S4b). In contrast to **KGF-29**, which exhibited an isolated 1D chain structure, **KGF-30** featured two-strand chain structures formed by interchain S...S interactions (3.271 Å) between 1D (–Cd–S–)_n chains. The S...S distance is smaller than the sum of the S–S vdW radii (3.60 Å). The two-strand chains were further assembled by weak vdW interactions (Fig. S5b).

Single crystals of **KGF-31** were obtained from Cd(NO₃)₂·4H₂O and *p*-HSPHOMe by solvothermal synthesis at 80 °C for 48 h. **KGF-31** crystallized in the orthorhombic *Iba2* space group (Table S1) containing two crystallographically non-equivalent Cd(II) ions (Fig. S1c), which both have [CdS₄] tetrahedral geometry and are coordinated by S atoms of *p*-SPhOMe ligands (Fig. S2c). The Cd–S bond lengths in **KGF-31** are similar to those in **KGF-29** and **KGF-30** (Table S2). All thiolate S atoms acted as μ_2 -S atoms (Fig. S3c), connecting adjacent [CdS₄] tetrahedra via repeated edge-

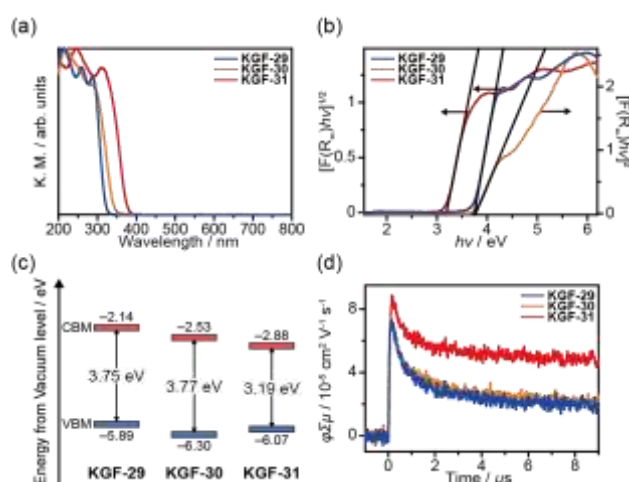


Fig. 2. Semiconductive properties of **KGF-29**, **KGF-30**, and **KGF-31**. (a) UV-Vis spectra, (b) Tauc plots, (c) energy diagram under vacuum level, and (d) TRMC spectra ($\lambda_{\text{ex}} = 355 \text{ nm}$).

sharing, thereby forming a 1D architecture composed of inorganic (–Cd–S–)_n chains along the *c*-axis. Notably, **KGF-31** featured three-strand chains formed by interchain S...S interactions (3.124 Å) that are significantly shorter than those in **KGF-30** (Fig. 1e, f, S3c). The resulting three-strand chain units were assembled by weak vdW interaction (Fig. S5c).

Accordingly, **KGF-29**, **KGF-30**, and **KGF-31** featured 1D structures with [CdS₄] tetrahedral geometries and inorganic (–Cd–S–)_n chains, in which X-ray photoelectron spectroscopy (XPS) revealed similar coordination environments (Fig. S6). Considering that Cd(II) S-CP with a non-substituted SHPh ligand formed a three-dimensional (3D) architecture,^{8a,b} the steric effect of OMe substituents may disturb the 3D extension of the network structure, leading to the formation of a 1D chain structure. Notably, the assembly of 1D chain structures is dependent on the position of the OMe substituents. **KGF-29** featured an isolated 1D structure, whereas **KGF-30** and **KGF-31** formed two- and three-strand chains, respectively, through interchain S...S interactions. The differences in the structures of these assembled chains may also be attributed to the steric effect of the OMe substituents. The OMe substituents in **KGF-29** are located near the 1D (–Cd–S–)_n chain and thus inhibit the formation of interchain S...S interactions, resulting in an isolated 1D structure. Conversely, **KGF-30** and **KGF-31** form two- or three-strand chains, respectively, via interchain S...S interaction because the OMe substituents are located farther from the 1D (–Cd–S–)_n chain, enabling the formation of interchain S...S interactions. Notably, the S...S distances observed in **KGF-30** and **KGF-31** are shorter than those obtained for conductive MOFs containing TTF-based ligands.¹¹ Optimized reaction conditions determined by tuning the reaction temperature and solvent afforded bulk powders of each phase (Experimental Section in the ESI). The purity of the obtained products was confirmed by powder X-ray diffraction (PXRD) and CHN elemental analyses (Fig. S7). Scanning electron microscopy (SEM) images also revealed that each compound has needle-like or rod-like morphology. The energy-dispersive X-ray spectroscopy (EDS) results are consistent with the predicted Cd:S ratio (Fig. S8).

The thermal stabilities of **KGF-29**, **KGF-30**, and **KGF-31** were evaluated by thermogravimetric (TG) analyses. The TG curves of **KGF-29**, **KGF-30**, and **KGF-31** show no apparent weight loss up to 240, 260, and 270 °C, respectively (Fig. S9). The chemical stabilities of **KGF-29**, **KGF-30**, and **KGF-31** toward distilled water, 0.1 M HCl aq., and 0.1 M NaOH aq. were also determined from the PXRD patterns of samples that had been immersed in the corresponding solvents for 24 h. The PXRD patterns remained unchanged after immersion (Fig. S10). The observed thermal and chemical stabilities may be attributed to the presence of strong Cd–S bonds.

The $(-Cd-S-)_n$ assembly formed by S...S interactions motivated us to investigate the semiconductive properties of the polymers. The optical band gaps of **KGF-29**, **KGF-30**, and **KGF-31** were evaluated by diffuse-reflectance ultraviolet-visible (DR-UV-Vis) spectroscopy. As depicted in Fig. 2a, **KGF-29**, **KGF-30**, and **KGF-31** exhibit UV absorption with absorption edges at 338, 366, and 392 nm, respectively. Based on the DFT calculation results (see following discussion), the optical band gaps were estimated assuming that **KGF-29** and **KGF-31** are indirect transition semiconductors and **KGF-30** is a direct transition semiconductor. The optical band gaps of **KGF-29**, **KGF-30** and **KGF-31** are 3.75, 3.77, and 3.19 eV, respectively (Fig. 2b and Table S3). The absolute valence band maximum (VBM) energy levels of **KGF-29**, **KGF-30** and **KGF-31** were -5.89 , -6.30 , and -6.07 eV below vacuum level, respectively, as determined by photoelectron yield spectroscopy (PYS) (Fig. S11). The absolute energies of the conduction band minimum (CBM) levels were estimated to be -2.14 , -2.53 , and -2.88 eV below the vacuum level calculated from the DR-UV-Vis spectra of **KGF-29**, **KGF-30**, and **KGF-31**, respectively (Fig. 2c). The differences in the energy levels may be attributed to the position of the OMe substituents. The presence of electron-donating OMe substituents in the *ortho*- and *para*-positions increased the VBM energy levels.

The photoconductive properties were characterized by time-resolved microwave conductivity (TRMC) measurements. TRMC is a non-contact technique that uses high-frequency electromagnetic waves to probe photoinduced transient conductivity to provide information on the dynamics of photogenerated charge carriers at the multi-nanometer scale. The $\varphi\Sigma\mu_{\max}$ (φ = quantum yield of charge carrier generation, $\Sigma\mu$ = sum of hole and electron mobility) values of **KGF-29**, **KGF-30**,

and **KGF-31** were 7.3×10^{-5} , 7.4×10^{-5} , and $8.8 \times 10^{-5} \text{ cm}^2 \text{ V}^{-1} \text{ s}^{-1}$, respectively (Fig. 2d). The effective lifetime (i.e., the weight-averaged lifetimes of double-exponential fits) of **KGF-29**, **KGF-30**, and **KGF-31** were determined to be 18.8, 22.7, and 68.4 μs , respectively (Fig. S12). Notably, **KGF-31** exhibits stronger TRMC signals and greater longevity than **KGF-29** or **KGF-30**. The $\varphi\Sigma\mu_{\max}$ values of **KGF-31** are relatively higher than those of the known photoconductive S-CPs (Table S4).

The photoconductive pathway was elucidated from first-principles calculations using the CASTEP software (details of the calculation method are given in the ESI). The calculations showed that **KGF-29** and **KGF-31** are indirect transition semiconductors, whereas **KGF-30** is a direct transition semiconductor. The calculated band gaps, (i.e., the energy difference between the VBM and CBM) in **KGF-29**, **KGF-30**, and **KGF-31** are 2.73, 3.01, and 2.50 eV, which are consistent with the trend obtained by DR-UV-Vis spectroscopy. The simulated band structures of **KGF-29** and **KGF-30** are relatively flat, with dispersion widths < 0.1 eV in the VBM and CBM. **KGF-31** also exhibits a flat band in the VBM but shows a steep dispersion in the CBM with a width of 0.32 eV. The direction of the CBM dispersion in **KGF-31** corresponds to the 1D structure (T-W and R-G) and therefore indicates that **KGF-31** exhibits high electron mobility along the 1D chain structure (Fig. 3). These mobile electrons would also facilitate long-lived charge-separated states on the conductive path. These results were in full accord with the TRMC results. Density of states (DOS) analysis provides further information about the elements that contribute to the formation of band structures. The partial DOS (PDOS) of **KGF-29** showed that the VBM mainly originated from the orbitals of C and S atoms, whereas the CBM largely consists of Cd (22.6%) and C (66.0%) atoms with a small contribution from S atoms (3.4%). C and S atoms also contribute significantly to the VBMs of **KGF-30** and **KGF-31**; however, the CBM of **KGF-30** is mainly composed of Cd (51.8%), S (18.9%), and C (28.4%), while that of **KGF-31** consists of Cd (68.7%), S (24.0%), and C (9.54%) (Table S5). The distribution of the VBM and CBM is in good agreement with the observed PDOS, wherein the VBM is localized on the SPhOMe ligand in all cases (Figs. S13–S15). However, the CBM of **KGF-30** and **KGF-31** is delocalized through the $(-Cd-S-)_n$ network (Fig. S14 and Fig. S15). These results demonstrate that the 1D $(-Cd-S-)_n$ chain strongly influences the electron mobility pathway. The high TRMC signal and long carrier lifetime

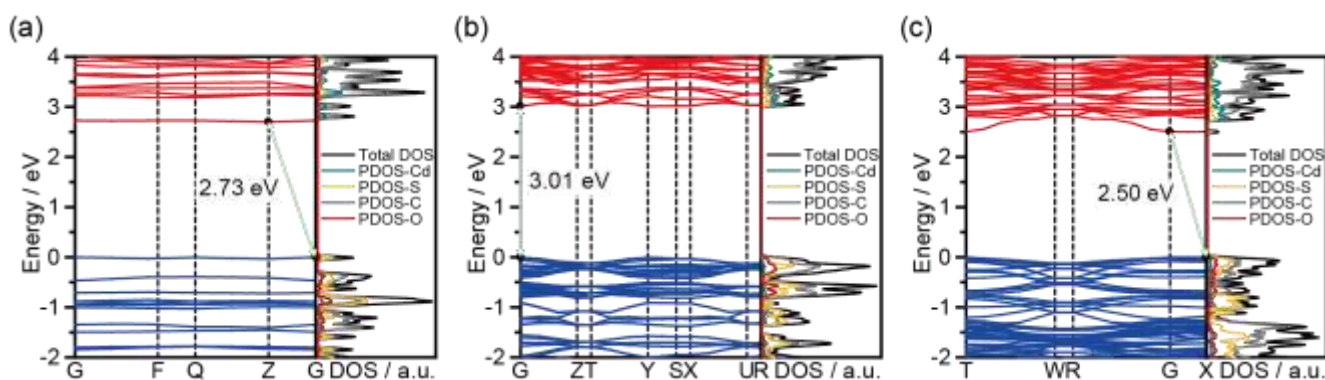


Fig. 3. Band structures and DOS profiles of (a) **KGF-29**, (b) **KGF-30**, and (c) **KGF-31**. VBM energy level is presented as zero.

observed in **KGF-31** may be attributed to the presence of the $(-Cd-S-)_n$ three-strand chains formed by S...S interactions. The distance of S...S contacts in conductive metal-organic frameworks with TTF-derived ligands significantly influences the resultant conductivity.^{11a,b} Hence, the interchain S...S interactions between 1D $(-Cd-S-)_n$ chains in **KGF-31** promote further charge delocalization, resulting in high photoconductivity and longevity. To date, investigations concerned with 1D semiconductive S-CPs have been extensively conducted on Cu(I)-based S-CPs systems, which tend to exhibit hole mobility.¹² In contrast, the Cd(II) S-CPs reported in this study exhibit electron mobility and therefore have potential applications for use in photocatalysts for H₂ production and CO₂ reduction, as well as optoelectronic devices.

In conclusion, we characterized the crystal structures and semiconductive properties of three 1D Cd(II) S-CPs [Cd(x-SPhOMe)₂]_n containing 1D $(-Cd-S-)_n$ chains. **KGF-29** featured an isolated 1D architecture, while **KGF-30** and **KGF-31** featured two- and three-strand chains assembled via interchain S...S interactions between inorganic $(-Cd-S-)_n$ chains. TRMC and first-principles calculations revealed that **KGF-31** exhibits high photoconductivity and longevity that originate from the three-strand $(-Cd-S-)_n$ chains. Our findings provide insights for the first time into the relationship between the $(-M-S-)_n$ assemblies in the crystal structure and the semiconducting properties. Future work in this area aims to synthesize two-dimensional arrangements of 1D Cd(II) S-CPs via S...S interactions and explore their potential applications.

This work was supported by JSPS Grant Numbers JP22K14702, JP20H05836, JP20H02577, JP23H01810, and JP23H04637 (Transformative Research Areas (A) "Supra-ceramics") and partially supported by the ENEOS Hydrogen Trust Fund. R. A. acknowledges financial support provided by the Izumi Science and Technology Foundation and Kawanishi Memorial ShinMaywa Education Foundation. D. T. acknowledges financial support provided by JST Grant Number JPMJPF2204. We thank Dr. M. Yoshida and Prof. M. Kato for the single crystal X-ray diffraction measurement. We would like to thank Editage (<http://www.editage.jp>) for English language editing.

Conflicts of interest

There are no conflicts to declare.

Notes and references

- (a) O. Veselska and A. Demessence, *Coord. Chem. Rev.*, 2018, **355**, 240; (b) J. Xie, L. Wang and J. S. Anderson, *Chem. Sci.*, 2020, **11**, 8350; (c) Y. Kamakura and D. Tanaka, *Chem. Lett.*, 2021, **50**, 523; (d) G. E. Wang, S. Luo, T. Di, Z. Fu and G. Xu, *Angew. Chem. Int. Ed.*, 2022, **61**, e202203151.
- (a) D. Dong, C. Yan, J. Huang, N. Lu, P. Wu, J. Wang and Z. Zhang, *J. Mater. Chem. A*, 2019, **7**, 24180; (b) Y. Kamakura, P. Chinapang, S. Masaoka, A. Saeki, K. Ogasawara, S. R. Nishitani, H. Yoshikawa, T. Katayama, N. Tamai, K. Sugimoto and D. Tanaka, *J. Am. Chem. Soc.*, 2020, **142**, 27;
- (c) Y. Kamakura, C. Suppaso, I. Yamamoto, R. Mizuochi, Y. Asai, T. Motohashi, D. Tanaka and K. Maeda, *Angew. Chem. Int. Ed.*, 2023, **62**, e202305923.
- (a) Y. Wen, G. E. Wang, X. Jiang, X. Ye, W. Li and G. Xu, *Angew. Chem. Int. Ed.*, 2021, **60**, 19710; (b) Y. Pan, C. Wang, Z. Fu, G. E. Wang and G. Xu, *Chem. Commun.*, 2022, **58**, 4615.
- (a) A. Pathak, J. W. Shen, M. Usman, L. F. Wei, S. Mendiratta, Y. S. Chang, B. Sainbileg, C. M. Ngue, R. S. Chen, M. Hayashi, T. T. Luo, F. R. Chen, K. H. Chen, T. W. Tseng, L. C. Chen and K. L. Lu, *Nat. Commun.*, 2019, **10**, 1721; (b) G. Xing, Y. Li, Z. Feng, D. J. Singh and F. Pauly, *ACS Appl. Mater. Interfaces*, 2020, **12**, 53841.
- (a) L. Sun, T. Miyakai, S. Seki and M. Dinca, *J. Am. Chem. Soc.*, 2013, **135**, 8185; (b) Y. Li, X. Jiang, Z. Fu, Q. Huang, G. E. Wang, W. H. Deng, C. Wang, Z. Li, W. Yin, B. Chen and G. Xu, *Nat. Commun.*, 2020, **11**, 261.
- (a) A. Kobayashi, E. Fujiwara and H. Kobayashi, *Chem. Rev.*, 2004, **104**, 5243; (b) J. L. Segura and N. Martin, *Angew. Chem. Int. Ed.*, 2001, **40**, 1372.
- C. B. Murray, D. J. Norris and M. G. Bawendi, *J. Am. Chem. Soc.*, 1993, **115**, 19, 8706.
- (a) D. Craig, I. G. Dance and R. Garbutt, *Angew. Chem. Int. Ed.*, 1986, **25**, 165; (b) C. Xu, H.-T. Shi, Z.-F. Xin, A.-Q. Jia and Q.-F. Zhang, *J. Clust. Sci.*, 2014, **25**, 1353; (c) H. Zhuang, L. Yang, J. Xu, F. Li, Z. Zhang, H. Lin, J. Long and X. Wang, *Sci. Rep.*, 2015, **5**, 16947.
- (a) C. Lavenn, L. Okhrimenko, N. Guillou, M. Monge, G. Ledoux, C. Dujardin, R. Chiriac, A. Fateeva and A. Demessence, *J. Mater. Chem. C*, 2015, **3**, 4115; (b) O. Veselska, N. Guillou, G. Ledoux, C. C. Huang, K. Dohnalova Newell, E. Elkaim, A. Fateeva and A. Demessence, *Nanomaterials*, 2019, **9**, 1408.
- W. Paritmongkol, T. Sakurada, W. S. Lee, R. Wan, P. Muller and W. A. Tisdale, *J. Am. Chem. Soc.*, 2021, **143**, 20256.
- (a) S. S. Park, E. R. Hontz, L. Sun, C. H. Hendon, A. Walsh, T. Van Voorhis and M. Dincă, *J. Am. Chem. Soc.*, 2015, **137**, 1774; (b) L. S. Xie, E. V. Alexandrov, G. Skorupskii, D. M. Proserpio and M. Dinca, *Chem. Sci.*, 2019, **10**, 8558; (c) J. Su, P. Cai, T. Yan, Z.-M. Yang, S. Yuan, J.-L. Zuo and H.-C. Zhou, *Chem. Sci.*, 2022, **13**, 1657.
- (a) C.-M. Che, C.-H. Li, S. S.-Y. Chui, V. A. L. Roy and K.-H. Low, *Chem. Eur. J.*, 2008, **14**, 2965; (b) Y. Zhang, T. Xia, K. M. Yu, F. Zhang, H. Yang, B. Liu, Y. An, Y. Yin and X. Chen, *ChemPlusChem*, 2014, **79**, 559; (c) H. Yan, J. N. Hohman, F. H. Li, C. Jia, D. Solis-Ibarra, B. Wu, J. E. P. Dahl, R. M. K. Carlson, B. A. Tkachenko, A. A. Fokin, P. R. Schreiner, A. Vaillonis, T. Roy Kim, T. P. Devereaux, Z.-X. Shen and N. A. Melosh, *Nat. Mater.*, 2017, **16**, 349.